X-ray Imaging of Shock Waves Generated by High-Pressure Fuel Sprays

Andrew G. MacPhee,[1] Mark W. Tate,[3] Christopher F. Powell,[1] Yong Yue,[2] Matthew J. Renzi,[3] Alper Ercan,[3] Suresh Narayanan,[1] Ernest Fontes,[4] Jochen Walther,[5] Johannes Schaller,[5] Sol M. Gruner,[3,4] Jin Wang[1]*

Synchrotron x-radiography and a fast x-ray detector were used to record the time evolution of the transient fuel sprays from a high-pressure injector. A succession of 5.1-microsecond radiographs captured the propagation of the spray-induced shock waves in a gaseous medium and revealed the complex nature of the spray hydrodynamics. The monochromatic x-radiographs also allow quantitative analysis of the shock waves that has been difficult if not impossible with optical imaging. Under injection conditions similar to those found in operating engines, the fuel jets can exceed supersonic speeds and result in gaseous shock waves.

High-pressure, high-speed sprays are an essential technology for many applications, including fuel injection systems, thermal and plasma spray coating, and liquid-jet machining (*1*–*4*). Liquid sprays are often difficult to record optically because of intense multiple light scattering from surrounding liquid droplets. In the case of fuel injection, an understanding of the structure and dynamics of the fuel sprays is critical to optimizing the injection process to increase fuel efficiency and reduce pollutants. Despite substantial advances in laser diagnostics over the past 20 years (*5*–*10*), the region close to the nozzle still has not yielded desired quantitative information. As a result, high-pressure fuel sprays have never been recognized as supersonic under typical fuel injection conditions (*11*, *12*). In this report, we use monochromatic x-radiography to probe the high-speed fuel sprays and show the generation of shock waves.

We studied a high-pressure common-rail diesel injection system typical of that in a passenger car with a specially fabricated single-orifice nozzle. The orifice was 178 μm in diameter, and the injection pressure could be set between 50 and 135 MPa. Fuel was injected into an x-ray–accessible spray chamber (*13*) filled with the inert gas sulfur hexafluoride (SF_6) at 1 atm pressure and room temperature (typically 30°C). This heavy gas allows simulation of the dense gas environment of a diesel chamber without resorting to high-pressure x-ray windows (*14*). The fuel was a blend of No. 2 diesel and an x-ray contrast–enhancing, cerium-containing compound, resulting in a total cerium concentration of 4 weight % (*15*).

We performed the time-resolved radiograph experiments on the fuel sprays by using two methods: (i) scanning with a focused, small x-ray beam and a fast point detector (avalanche photodiode, APD), in a line-of-sight manner (*13*), at bending magnet beamline 1-BM at the Advanced Photon Source (APS) and (ii) using a beam of 1% band pass and extended size along with a microsecond framing area detector, the Cornell Pixel Array Detector (PAD) (*16*, *17*), at the D-1 beamline of the Cornell High Energy Synchrotron Source (CHESS). The area detection method was the only practical technique with which to visualize the shock waves induced by the fuel spray.

For single-wavelength x-rays, the analysis of the transmission of the attenuating material (the fuel) gives an exact measure of the mass in the x-ray beam (*18*). There was a distinct boundary between the ambient gas and the leading edge of the fuel spray, as indicated by the abrupt increase in fuel mass from 0 to nearly 5 μg at $t = 0.17$ ms for data taken 1 mm from the injector nozzle (Fig. 1A). The sharpness of the interface facilitated the calculation of the apparent speed of the leading edge (Fig. 1B). A highly concentrated fuel region immediately followed the leading edge represented by an extremely sharp peak, which was caused by accumulation of droplets as they impacted on the ambient gas at the leading edge (*19*). Although the injection pressure inside the nozzle remained stable (within 5% of 50 MPa) during the injection (*20*),

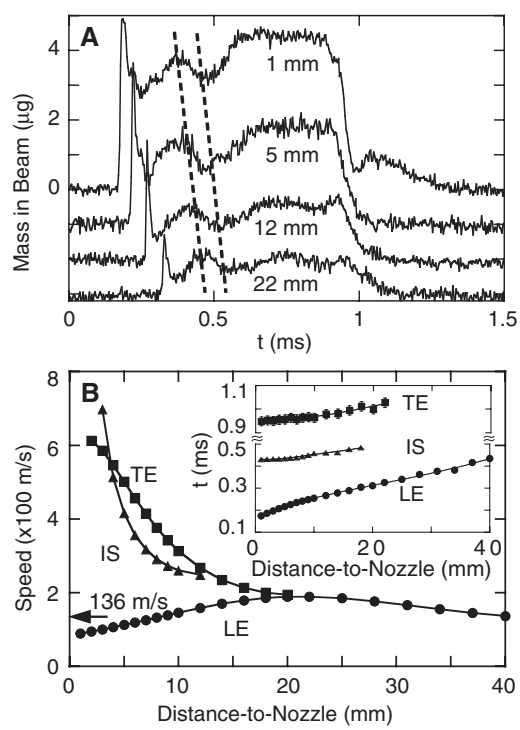

Fig. 1. Dynamics of the high-pressure fuel sprays measured with the point-by-point scanning method: (**A**) time evolution of the integrated fuel mass in the x-ray beam on the spray axis at 1, 5, 12, and 22 mm from the nozzle and (**B**) the calculated spray speeds. The data in (A) were collected by positioning the transient fuel spray between the x-ray beam (focused and collimated to 500 μm horizontal (H) by 50 μm vertical (V), full width at half maximum, and tuned to 6.0 keV) and an APD and by recording the time-resolved response of the detector with a fast digitizing oscilloscope. Each curve is the average of 100 injection cycles to improve the signal-to-noise ratio. Repeated experiments demonstrated that the data were well reproducible. Each data point spans a time interval of 3.68 μs, which is the fundamental period of the APS synchrotron storage ring. The fuel injection pressure was 50 MPa, and the injection duration was about 800 μs. The four curves are each shown as displaced vertically by 1 μg for clarity. The speed values for the leading edge (LE) and trailing edge (TE) were calculated by the derivative of their penetration curves shown as the inset in (B). By tracking the distinctive features such as the spray internal segment (IS) between the two marker lines in (A), the speed of the segment was evaluated with the correlation method illustrated in (*21*).

[1]Advanced Photon Source and [2]Energy System Division, Argonne National Laboratory, Argonne, IL 60439, USA. [3]Department of Physics and [4]Cornell High Energy Synchrotron Source, Cornell University, Ithaca, NY 14853, USA. [5]Corporate Research, Robert Bosch GmbH, 70049 Stuttgart, Germany.

*To whom correspondence should be addressed. E-mail: wangj@aps.anl.gov

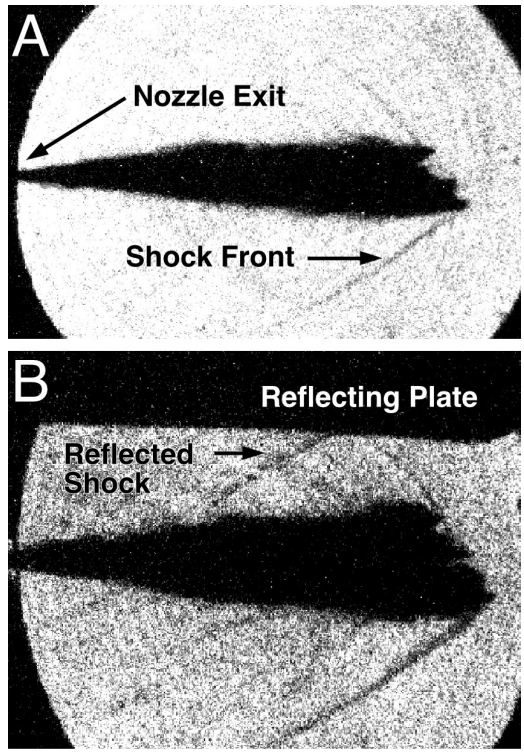

Fig. 2. Optical Schlieren images of the shock waves generated by fuel sprays in SF_6 gas collected with the injection pressure set at 80 MPa (**A**) and the effect of a reflecting wall to the shock front (**B**). The spray propagates from left to right along the axis of the injector in the imaging field. To visualize the density change in the shock front in the gas medium, we collimated flashed white light beam by an aperture and a collimating lens before illuminating the fuel sprays. The images were collected at the Schlieren plane. The exposure time was controlled by a gated image intensifier to a duration of about 0.1 μs. The bright circle in the images indicates the size of the observation window of the test chamber, measured at 25 mm in diameter. The imaging magnification in (B) was set slightly higher than that in (A) to emphasize the region where the reflection of the shock front occurred. The portion of the spray visualized here is the optically dense, low-mass cloud of droplets surrounding the thin, main fuel jet that can only be imaged by x-rays.

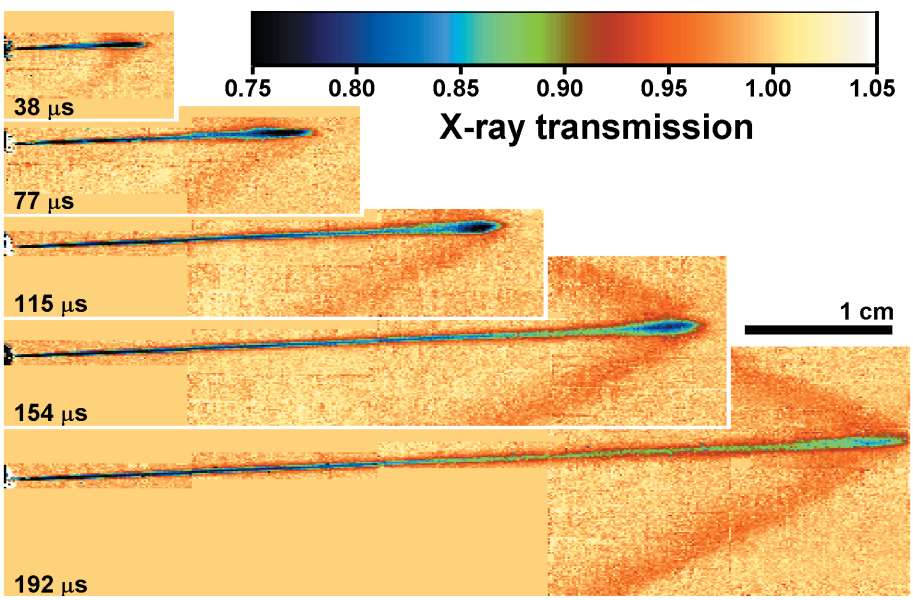

Fig. 3. Time-resolved radiographic images of fuel sprays and the shock waves generated by the sprays for time instances of 38, 77, 115, 154, and 192 μs after the start of the injection (selected from the total of 168 frames taken). The imaged area shown in the largest panel is 61.7 mm (H) by 17.5 mm (V) with data corrected for the divergence of the x-ray beam. Because the x-ray beam size in the experiment was 13.5 mm (H) by 2.5 mm (V), the imaged area was built up by shifting the position of the injector relative to the beam and the PAD and repeating the injection cycle. Boundaries between these areas can be seen upon close inspection. The exposure time per frame was set to 5.13 μs (twice the CHESS synchrotron period) with subsequent images taken after an additional 2.56-μs delay. Each position shown is the average of images from 20 fuel injection cycles. The detector was not positioned over all possible areas of the image, so specific images show missing areas. To optimize the conditions for the direct visualization of the shock waves, we chose the injection pressure to be 135 MPa. The contrast of the shock wave was low, corresponding to only an average of about 15% increase in gas density near the shock front. Therefore, the false-color levels of the images have been set to accentuate small differences in the x-ray intensity arising from the slightly increased x-ray absorption in the compressed SF_6 gas. The progression of the shock wave can be seen much more clearly in the "movie" of successive frames (*26*).

the fuel mass in the spray body appeared to fluctuate with rather large amplitudes partly because of the traveling shock waves generated by the impact (*21*). By 1 ms, a well-defined spray trailing edge was also observed, indicating that the injection event had finished. The trailing edge of the spray illustrates the dynamics of the injection process because it moves at an instantaneous speed much greater than that of the leading edge in the region close to the nozzle (Fig. 1B). The trailing edge speed can be greater than 600 m/s as the spray exits the nozzle, well above the sonic speed in SF_6 of 136 m/s (*22*). Thereafter, the trailing edge slows to 180 m/s at 20 mm from the nozzle, roughly equal to the leading edge speed.

We used the density fluctuations shown in the time-resolved mass profiles (Fig. 1A) to perform correlation calculations and determine the internal speed of the spray body (*23*). The calculated speed of the spray segment included within the two markers shown in Fig. 1A lies between the speeds for the leading and trailing edges but is much closer to that for the trailing edge (Fig. 1B), suggesting that the internal part of the spray travels much faster than the sonic speed in SF_6. Although these point-by-point measurements strongly indicated that the fuel spray should generate shock waves, such a method lacked spatial coverage and became impractical to directly image the shock waves.

To confirm the supersonic nature of the sprays, we visualized the shock waves in the same spray system by optical Schlieren imaging of visible light (*11*, *24*, *25*) when the injection pressure reached 80 MPa, as shown in Fig. 2A. A reflecting wall was also introduced in the testing chamber. The shock front was reflected off this wall and impinged back onto the spray (Fig. 2B). The influence of the reflected shock front on the appearance of the spray was not determined with statistical significance. As expected, the optical images yielded only the cone angle of the shock wave.

We used high-intensity synchrotron x-ray sources and the PAD to image the shock waves (*26*). As shown in Fig. 3, in an experiment where the fuel injection pressure was set to 135 MPa, the leading edge speeds reached 345 m/s and exceeded the sonic speed upon emergence. The shock wave front, or the so-called Mach cone, emanated from the leading edge of the fuel jet soon after emergence with an increase in x-ray absorption of up to 3% on the cone. The Mach cone angles were also measured at each instance, and the values agreed well with the leading edge speed.

We also derived the mass density distribution of gas medium near and inside the

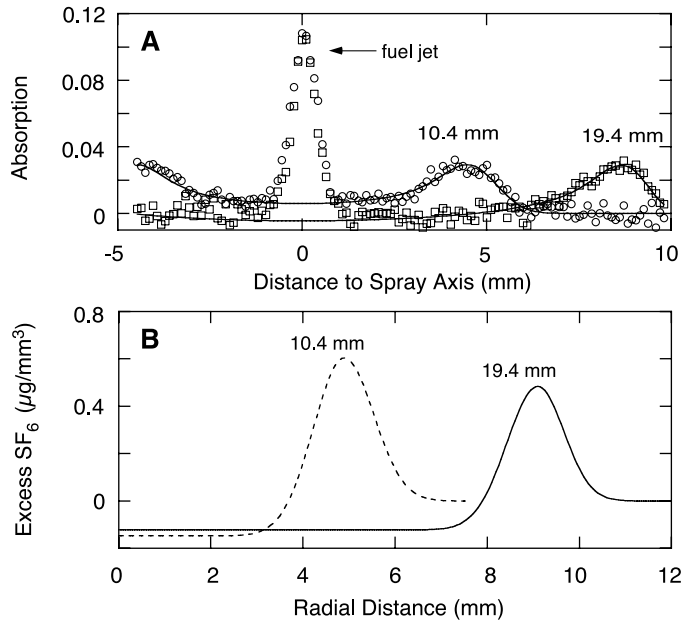

Fig. 4. Quantitative analysis of the radiographic images of the Mach cone: (**A**) deconvolution of the absorption data by the line-of-sight calculation and (**B**) best fitting models of density distribution of excess ambient gas near the Mach cone. In (A), absorption curves were generated from a two-dimensional image (last panel of Fig. 3) in a direction normal to the fuel jet direction at positions of 10.4 mm (circles) and 19.4 mm (squares) behind the spray tip, which traveled to 60 mm from the nozzle. The peak in each of the curves at 0 mm is due to absorption in the fuel jet, whereas the peaks near 4 mm (circles) and 9 mm (squares) are from the Mach cone. The solid curves are numeric fits to axially symmetric gas density models (B). This numerical model is an asymmetric Gaussian distribution across the Mach cone with nearly uniform densities inside and outside the shell of the cone. All image data include about 2-mm spatial smearing due to the 5-μs time resolution of the image (*29*) and to the possible multiple shock fronts near the spray tip (see Fig. 2).

Mach cone, as shown in Fig. 4. In the plane perpendicular to the jet axis, the shocked region is a cone with an excess density in the SF_6 of about 0.6 μg/mm^3 measured at 10.4 mm from the spray tip. Behind the high-density region, the interior of the cone has a small but observable reduction in the gas density from the ambient (Fig. 4B), which implies that decompression has occurred away from the Mach cone. Although there is no simple hydrodynamic interpretation to explain the observation, this behavior is different from the compression shock waves generated by a rigid object (*27*).

The manner in which the shock waves affect the atomization of the fuel and the combustion processes is currently unknown. With more injection systems adopting preinjection technology (a short pilot injection before main injection), the engine cylinders are likely to be filled with fuel vapor-air mixture under high temperature before the main spray arrives. It has been recognized that the mixture would have a sonic speed lower than that of either fuel vapor ($<$130 m/s at room temperature) or air, so the generation of shock waves by the main fuel injection should not be surprising, even at elevated engine operating temperature. In this regard, the presence of the dense fill gas used in our study (SF_6) mimics this injection condition. This study has paved the way to directly study the complete range of fluid dynamics inside and close to high-pressure liquid sprays. The time-resolved x-radiographic method should also prove useful in characterizing highly transient phenomena in optically dense materials, such as dense plasma and complex fluid-gas interactions.

References and Notes

1. J. D. O'Keefe, W. W. Wrinkle, C. N. Scully, *Nature* **213**, 23 (1967).
2. K. Kuo, Ed., *Recent Advances in Spray Combustion: Spray Atomization and Drop Burning Phenomena* (Americon Institute of Aeronautics and Astronautics, Reston, VA, 1996), vols. 1 and 2.
3. H. Herman, *MRS Bull.* **13**, 60 (1988).
4. R. A. Tikhomirov, V. F. Babanin, E. N. Petukhov, I. D. Starikov, V. A. Kovalev, *High-pressure Jetcutting* (ASME Press, New York, 1992).
5. N. Chigier, *Prog. Energy Combust. Sci.* **17**, 211 (1991).
6. A. J. Yule, A. P. Watkins, *Atomization Sprays* **1**, 441 (1991).
7. R. J. Adrian, *Annu. Rev. Fluid Mech.* **23**, 261 (1991).
8. W. Hentschel, K.-P. Schindler, *Opt. Lasers Eng.* **25**, 401 (1996).
9. Z.-M. Cao, K. Nishino, S. Mizuno, K. Torii, *JSME Intl. J. Ser. B* **43**, 582 (2000).
10. Y.-Y. Zhang, T. Yoshizaki, K. Nishida, *Appl. Opt.* **39**, 6221 (2000).
11. T. Nakahira, M. Komori, N. Nishida, K. Tsujimura, in *Shock Waves*, K. Takayama, Ed. (Springer-Verlag, Berlin, 1992), vol. II, pp. 1271–1276.
12. H.-H. Shi, K. Takayama, O. Onodera, *JSME Intl. J. Ser. B* **37**, 509 (1994).
13. C. F. Powell, Y. Yue, R. Poola, J. Wang, *J. Synchrotron Rad.* **7**, 356 (2000).
14. SF_6, a heavy gas with molecular weight of 146, was used to simulate the relatively dense ambient gas environment in a diesel engine during the adiabatic compression part of the engine cycle when the diesel fuel is normally injected. The sonic speed in SF_6 at room temperature (30°C) is 136 m/s (*22*), considerably less than the 330 m/s speed of sound in air at the same temperature. Fuel sprays with much higher speeds can be generated at the higher injection pressures used in diesel engines.
15. The cerium additive (DPX9, Rhodia Terres Rares) was included to increase the x-ray absorption of the fuel jet and accounted for about 50% of the total absorption at the selected x-ray energy.
16. S. L. Barna *et al.*, *IEEE Trans. Nucl. Sci.* **44**, 950 (1997).
17. G. Rossi *et al.*, *J. Synchrotron Rad.* **6**, 1096 (1999).
18. Radiography with polychromatic x-ray beams was reported previously to study liquid jets (*28*). However, lack of quantitativeness seriously limited its capability of imaging and characterizing high-pressure fuel sprays. For monochromatic x-rays transmitting through a nonuniformly distributed material, the analysis of the transmission of the attenuating material is given by $I/I_0 = \exp(-\mu_M M)$, where I and I_0 are the transmitted and incident x-ray intensities, respectively, μ_M is the mass absorption coefficient, which can be measured and calibrated accurately for the absorbing medium (fuel) at the single wavelength, and M is the mass of fuel in the beam. Thus, the time evolution of the measured x-ray transmission I/I_0 can be simply transformed into integrated, line-of-sight fuel mass data at each point in the radiograph.
19. Because the spray is composed of an aerosol of streams and droplets, the liquid at the leading edge of the spray can move at rates quite different than those of the average body of the spray. Without the resistance or impact to the ambient gas, the spray body can move much faster than the leading edge and with speeds close to that for the trailing edge. This large speed variation can also cause accumulation of the fuel near the tip. Instantly after the nozzle opening, the high fuel concentration in the spray tip is certainly caused by the transient nature of the fuel pressure in the nozzle.
20. The injection pressure was measured both inside the nozzle and in the common rail with the same injection system and with a similar nozzle (minisac type).
21. A shock generated by the impact of the fuel spray on the ambient gas travels within the spray body as a compressed gaseous pocket resulting in a low–fuel density region.
22. J. J. Hurly, D. R. Defibaugh, M. R. Moldover, *Intl. J. Thermophys.* **21**, 739 (2000).
23. The correlation function is defined by $g(x,\Delta x,t) = \int M(x,\tau)M(x+\Delta x, \tau+t)d\tau$, where x is the coordinate along the spray axis, Δx is a small displacement at which another time-resolved mass profile data set was taken, and t is the elapsing time. For practical purposes, Δx can be 1 mm. When this correlation function is calculated with a small fraction in the mass time-evolution data, such as those indicated within the two markers shown in Fig. 1A, one obtains a peak value in the correlation function at $t = \Delta t$. Therefore, the speed of such a fraction of the spray at the location x can be estimated by $v(x) = \Delta x/\Delta t$.
24. E. Hecht, *Optics* (Addison-Wesley, Reading, MA, ed. 3, 1998).
25. J. E. Field, M. B. Lesser, *Proc. R. Soc. London Ser. A* **357**, 143 (1977).
26. X-radiographic images of shock wave propagation are available in the form of animation on *Science* Online at www.sciencemag.org/cgi/content/full/295/5558/1261/DC1.
27. P. A. Thompson, *Compressible-Fluid Dynamics* (McGraw-Hill, New York, 1971).
28. J. M. Char, K. K. Kuo, K. C. Hsieh, *J. Propuls. Power* **6**, 544 (1990).
29. The 5-μs time resolution was a combination of the image integration time and jitter associated with synchronizing the image integration and the injection cycles. The electronic timing jitter was less than 300 ns.

30. We thank R. Poola for his initiation and participation of the research, R. Cuenca and A. McPherson for their technical support, and M.-C Lai and O. Vasilyev for discussions. Beamline support at CHESS and the APS is gratefully acknowledged. This work, the use of the APS, and the PAD development are supported by the U.S. Department of Energy under contract W-31-109-ENG-38, the Freedom CAR Program, and grants DE-FG-0297ER14805 and DE-FG-0297ER62443. CHESS is supported by the U.S. NSF and the NIH under award DMR-9713424.

16 November 2001; accepted 11 January 2002